Zheng Chen[1]
Richard Graham[1*]
Mark A. Burns[1, 2]
Ronald G. Larson[1]

[1]Department of Chemical Engineering, The University of Michigan, Ann Arbor, MI, USA
[2]Department of Biomedical Engineering, The University of Michigan, Ann Arbor, MI, USA

Received October 24, 2006
Revised February 11, 2007
Accepted February 12, 2007

Research Article

Modeling ssDNA electrophoretic migration with band broadening in an entangled or cross-linked network

We use a coarse-grained model proposed by Graham and Larson based on the temporary network model by Schieber *et al.* [1] to simulate the electrophoretic motion of ssDNA and corresponding band broadening due to dispersion. With dimensionless numbers reflecting the experimental physical properties, we are able to simulate ssDNA behavior under weak to moderate electric field strengths for chains with 8–50 entanglements *per* chain (~1000–8500 base pairs), and model smoothly the transition from reptation to oriented reptation. These results are fitted with an interpolation equation, which allows the user to calculate dimensionless mobilities easily from input parameters characterizing the gel matrix, DNA molecules, and field strengths. Dimensionless peak widths are predicted from mobility fluctuations using the central limit theorem and the assumption that the mobility fluctuations are Gaussian. Using results from previous studies of ssDNA physical properties (effective charge ξq and Kuhn step length b_K) and sieving matrix properties (pore size or tube diameter a), we give scaling factors to convert the dimensionless values to "real" experimental values, including the mobility, migration distance, and time. We find that the interpolation equation fits well the experimental data of ssDNA mobilities and peak widths, supporting the validity of the coarse-grained model. The model does not account for constraint release and hernia formation, and assumes that the sieving network is a homogeneous microstructure with no temperature gradients and no peak width due to injection. These assumptions can be relaxed in future work for more accurate prediction.

Keywords:
Brownian dynamics / Coarse-grained model / Mobility / Peak width / ssDNA
DOI 10.1002/elps.200600684

1 Introduction

Electrophoretic separation is a widely used technology for separating polyelectrolytes, principally based on their size, flexibility, and charge. This method has been used for size fractionation of biological molecules including oligonucleotides, nucleic acids, peptides, genomic DNA, and proteins. One common property of these molecules is that they possess ionizable groups and so are able to migrate either to the cathode or to the anode when they are charged at suitable pH values. They are usually macromolecules, so that their migration behavior is not only affected by thermal motion but also by their molecular conformations and interactions with the separation medium. Analysis of electrophoretic behavior must seek to account for all of these aspects. For instance, DNA electrophoresis is well known to be affected by the electric field, the DNA size, the base sequence, the sieving matrix, the pH, the running temperature, and other factors.

Theoretical studies of DNA electrophoresis over the past few decades [2–4] have greatly improved our understanding of the process, and thereby led to new methods of separation such as PFGE. The early "biased reptation" theory, initially developed for polymers encountering obstacles [5, 6] and then used for DNA gel electrophoresis by Slater and Noolandi [7], envisions snake-like migration of long-chain DNA molecules through an entangled polymer network. It predicts power law dependences of DNA migration rate on DNA size and electric field that are close to what is observed experimentally. Later, the "biased reptation with fluctua-

Correspondence: Professor Ronald G. Larson, Department of Chemical Engineering, The University of Michigan, Ann Arbor, MI 48105, USA
E-mail: rlarson@umich.edu
Fax: +1-734-763-0459

Abbreviations: BRF, biased reptation with fluctuation; **BRW,** biased reptation worm-like; **LPA,** linear polyacrylamide; **PA,** polyacrylamide; **PDMA,** poly(N,N-dimethylacrylamide)

* Current address: School of Physics and Astronomy, University of Leeds, Leeds LS2 9JT, UK.

tions" (BRF) model [3] introduced chain end fluctuations, enabling it to explain most of the qualitative observations of DNA migration under an electric field and even give quantitative predictions for low fields.

The reptation theory, especially the BRF theory, has been widely incorporated into various simulation schemes, including the lattice model by Barkema *et al.* and Heukelum *et al.* [8–10], the bead and spring model (also called Rouse and Zimm model) by Smith *et al.* [11], and the more recent tube models incorporating internal modes. "Tube models" with internal modes represent the properties of the sieving media and the dynamic behavior of DNA chain more realistically than simpler reptation models that ignore internal modes such as thermally driven fluctuations of the chain contour length or chain extension due to the electric field. Examples of tube models with internal modes include the "repton model" by Duke [4] and the "lakes-straits" model by Zimm [12]. While representing a step towards more realism, these models have their own limitations; for instance, both the Brownian diffusion between neighboring "lakes" and the electric force exerted on the lakes were ignored in the lakes-straits model. The recently proposed model by Graham and Larson [13], which applies the temporary network model of Schieber *et al.* [1] to electrophoresis, overcomes some of these limitations, and thus it is the basis for the ssDNA electrophoresis simulation discussed in this paper.

To evaluate the quality of a separation, two factors are typically used as measures of either the resolving power or the efficiency, namely resolution (R_s) and the number of theoretical plates (N_p), respectively. N_p is a measure of peak width or width at half maximum (hw) in the separation, which is a dispersion characteristic of a single molecular component. More recently, both Oda and Landers [14] and Heller [15] have suggested that the number of theoretical plates is not the best measure of the size fractionation capability of an electrophoretic separation, but instead the resolution is more appropriate, since it includes information on both peak width and peak spacing. As defined in Eq. (1) below, calculation of resolution incorporates the peak spacing in the term $(\Delta\mu/\mu_{av})$ and the peak width in the term N_p, where μ_{av} is the average mobility, $\Delta\mu$ is a measure of its variability, and $N_2 - N_1$ gives the size difference of DNA molecules, where N is the number of bases in the molecule. Experimentally, the resolving power has been observed to become poor when sequencing ssDNA of sizes above 1 k, although up to 1200 base pairs have been sequenced over a long separation distance of 40 cm and a time of 60 min by Chu and co-workers [16], and a read length of 1300 base pairs has been achieved in 2 h by Zhou *et al.* [17]. Determining the maximum chain size that can be resolved in a given distance, and under which conditions, is one of the major goals of research into electrophoretic separation.

$$R_s = \frac{1}{4\left(N_2 - N_{1)}\right)}\left|\frac{\Delta\mu}{\mu_{av}}\right| N_p \qquad (1)$$

In this paper, we focus on ssDNA electrophoretic behavior in either entangled polymer solutions or cross-linked gels and give a semiquantitative prediction of resolution for various conditions. While most of the studies of DNA migration behavior have focused on dsDNA, separation of ssDNA gives more important genomic information, such as single nucleotide mutations, genomic coding, polymorphism, *etc.* Experimental data for the separation of ssDNA are insufficient, especially for molecules larger than 1000 base pairs. In 1994, Manabe *et al.* [18] showed that ssDNA oligonucleotides up to 500 bases in length can be sequenced under a field of 200 V/cm over an effective distance of 50 cm using a 9% noncross-linked polyacrylamide (PA), a medium with estimated tube diameter less than 2 nm (Table 3), comparable to the persistence length of ssDNA. In addition, they predicted the resolution of their CE system by linearly extrapolating the plot of peak position *vs.* base number, and found poor resolution ($R = 0.11$) for DNA sizes longer than 600 base pairs. Slater and Drouin [19] also pointed out the impossibility of sequencing ssDNA with lengths of thousands of bases with PA. However, the resolution predicted in this previous study was much lower than what was later achieved by an alternative sieving media (a mixture of linear polyacrylamide (LPA) and poly(*N*,*N*-dimethylacrylamide) (PDMA)), which can successfully sequence DNA (one-color) up to 1200 base pairs ($R = \sim 0.3$) over a distance of only 40 cm [16], or can realize four-color sequencing with read lengths up to 1300 base pairs ($R = \sim 0.3$) using an LPA mixture with two different molecular weights [17]. Although these advancements have taken years to achieve, their attainment shows the possibility of further improvement in DNA separation.

Computer-based prediction of DNA migration and resolution would provide a rapid way to select semioptimized conditions on which experiments can be focused. So far, however, most theoretical work has been limited to the prediction of DNA mobility alone, lacking a systematic study for the prediction of resolution, although the reptation theory has given a scaling estimate for the dispersion coefficient. In this work, we simulate both the average DNA mobility and fluctuations around this average (*e.g.*, variance), and then use these to determine resolution by exploiting the central limit theorem. The goal is to develop a semiquantitative tool to help in designing optimum sieving media and running conditions for DNA electrophoresis.

To construct such an easy-to-use algorithm with tunable parameters taken from real experimental conditions, we use a tube model based on a coarse-grained algorithm, which has similarities to the tube models developed earlier. In this picture, a long DNA molecule threads through a highly entangled network, by sliding in the tube between topological constraints in the medium. New entanglement segments are generated by the chain "head", which selects its direction stochastically, biased towards the field direction. Thus, new tube segments are created and oriented along the field direction. And once chosen, a new tube segment constrains the chain as it creeps through the network. Thus, over short

time scales, the polymer chain only fluctuates within the tube, while over a longer time-scale, the polymer moves into a new constraining tube [6]. In the model of Graham and Larson, the DNA dynamics are governed by the chain free energy (F_s in Eq. 2), which is modified from what was used by Schieber *et al.* in 2003 [1] to include both chain finite extensibility (the first four terms on the right of Eq. 2), and the contribution from the external electric field (the last term on the right of Eq. 2). The finitely extensible free energy is obtained by integrating an approximation of the inverse Langevin function [20]. The entanglement destruction probability and the mobility matrix are revisions from the Schieber model, as described in the paper by Graham and Larson [13].

$$\underbrace{\frac{F_s}{K_B T}}_{\text{Chain free energy}} = \underbrace{\frac{Q_s^2}{2N_s b^2} - N_s \ln\left[1-\left(\frac{Q_s}{bN_s}\right)^2\right] + \frac{3}{2}\ln\left(\frac{2\pi N_s b^2}{3}\right)}_{\text{Finitely extensible free energy}} + \underbrace{\ln N_e}_{\text{Chemical potential of one segment}} \underbrace{- \xi q E\left(R_x^{s-1} + \frac{1}{2}Q_s \cos\theta\right) N_s}_{\text{Electric field contribution}} \quad (2)$$

A virtue of this new model is its ability to simulate the full distribution of DNA migration rates across a wide range of field strengths spanning from reptation to oriented reptation up to the point at which the mobility reaches unity. We thus cover the crossover regime between reptation and oriented reptation, and use the model to predict both electrophoretic mobility and separation resolution.

2 Results and discussion

2.1 ssDNA physical properties

The migration behavior of ssDNA molecules is determined by the properties of both the migrating DNA molecules and the surrounding gel matrix or polymer solution. Although there have been many investigations of the migration behavior of dsDNA, the migration behavior of ssDNA has been much less studied. In comparison with dsDNA, ssDNA is more flexible since its persistence length (p) is only around 2.6–4.4 nm at an ionic strength of ~0.01, while that of dsDNA is around 50 nm at the same ionic conditions [21]. Here, the persistence length is estimated from the relationship $2pL = 6R_g^2$, where L is the molecular contour length and R_g is the radius of gyration, which is in turn estimated from the hydrodynamic radius R_h using a known value of R_h/R_g. A value of p = 2.6 nm is obtained from the theoretical value of $R_h/R_g = 0.664$ for the non-free-draining regime, while p = 4.4 nm is obtained from $R_h/R_g = 0.5$, which is based on the measurements using monodisperse dsDNA by Tinland *et al.* [21]. Most of the ssDNA electrophoresis experiments referred to in this paper were carried out in a 0.5 × Tris-borate-EDTA (TBE) buffer solution, whose ionic strength was calculated to be around 0.026 M by Mohanty and Stellwagen [22]. Therefore, in the following section, we will take the Kuhn step length (b_K, twice the persistence length) to be 5 nm, which is approximately the value for ssDNA chains in a solution of ionic strength I = 0.026 M with $R_h/R_g = 0.5$, as calculated using the equation given in reference [21]. We also assume that the electric force, due to each segment residing in the pore, acts at the center of the "pore" or tube segment, except in the case of the end segment, for which the electric force is positioned at the end entanglement point, bounding the end segment. Each Kuhn segment of the polymer is assumed to carry an equal fraction of the drag [13].

The effective charge *per* Kuhn step of ssDNA, ξq, is determined from measurements on dsDNA [23], giving approximately $-30 \pm 10e$ *per* Kuhn step for dsDNA in a 0.5 × TBE solution [23]. The properties of ssDNA and dsDNA are listed in Table 1, including ξq for ssDNA, which we will estimate in what follows to be $\xi q^{ss} = -0.6e$ for the experimental conditions considered here (I = 0.026 M). This value will be used in Section 2.3 to determine the relationship between the reduced field used in the simulation and the real value used in experiments. The definition of the reduced field (Section 2.3, Eq. 8) allows us to compare a single set of simulation results to experimental results for various electrophoresis systems with different electric fields and different sieving media if they have equal values of the dimensionless numbers governing the process (see below). Note that the effective charge *per* Kuhn step that we use here is much less than the bare value derived from one electron charge *per* base or two *per* base pair, assuming fully ionized phosphate groups. However, it is well known that these charges are neutralized to a degree that depends on the ionic strength, and that the net charge also affects the effective persistence length of the DNA molecule [21, 24]. Physical properties of both ssDNA and dsDNA in Table 1 will be used in the following sections to convert our simulated results to corresponding experimental ones.

The radius of gyration, which was used to calculate the persistence length by Tinland *et al.* [21], depends on chain length and polymer flexibility, as shown in Table 2 [35]. For a semiflexible chain with $L >> b_K$ (valid for dsDNA longer than about 3000 base pairs, and for ssDNA longer than around 100 bases), we can simplify the equation proposed by Oberthur [26] to

$$R_g^2(M) = \frac{Lb_K}{6} - \frac{9}{48}b_K^2 \quad (3)$$

where b_K is the Kuhn step length, and L is the extended chain length (*i.e.*, contour length). Furthermore, for ssDNA, the Kuhn step length (b_K) is around 5 nm and the length of one nucleotide (b_0) is 4.3 Å. The Kuhn step length for dsDNA is 100 nm and b_0 is 3.4 Å. Therefore, we have the following expressions derived from above Eq. (3), where N is the number of bases or base pairs.

$$R_g^{2,ss}(\text{nm}^2) = 0.358N - 4.69 \quad (4)$$

Table 1. Comparison of physical properties of ssDNA and dsDNA

Physical properties	ssDNA	dsDNA
Length *per* base/base pair (b_0)	4.3 Å [25]	3.4 Å
Persistence length (p)	2.58–4.41 nm when I = 0.01 M [21]	50 nm when I = 0.01 M [23]
Effective charge *per* Kuhn step, ξq	$-0.6e$ (as calculated with Eq. 10) Charge *per* base = $-0.05e$	$-30e$ [23]
Radius of gyration squared, $R_g{}^2$ (nm^2)	0.358 N [26] (See Section 2 and Eq. 3)	5.66 N [26] (See Section 2 and Eq. 4)
Free solution mobility, (cm^{2}V^{-1}s^{-1})	1.03–1.04 [27] (15-mers, random sequence, endtagged fluorescent dye, high ionic strength, 10 × TBE, high field, ~600 V/cm) 1.83 [28] (size-independent mobility) 2.8–5.4, [29], [30], [31] (Ref. [30]: poly(dT)$_n$ in various salt solutions of ionic strength I = 0.1, 0.01, and 0.001 M; ref. [31]: ssDNA in 40 mM TAE buffer) or μ_0 (I) = (3.16 − 5.32 I + 2.91 I^2) × 10^{-4} (I is in units of M [32], in an APS solution with 3 M urea) 3.8 ± 0.1(oligomers, free solution mobility is an extrapolated value at 0%T in the plot of mobility *vs.* gel concentration) [33]	1.14 [27] (15-mers, random sequence, endtagged fluorescent dye, high ionic strength, 10 × TBE, high field, ~600 V/cm) 3.75 ± 0.04 (in TAE buffer) 4.5 ± 0.1 (in TBE buffer) [34]

TAE, Tris-acetate-EDTA

$$R_g^{2\,ds}(\mathrm{nm}^2) = 5.67N - 1875 \quad (5)$$

The second term in both equations can be ignored when the chain is long enough to be considered Gaussian ($R_g^2 \propto L \propto N$). This approximation is only valid for ssDNA larger than 130 base pairs and dsDNA larger than 3300 base pairs (error $\leq$ 10%).

2.2 Characterization of sieving matrices

The electrophoretic behavior of a DNA chain depends not only on its own properties but also on the properties of the sieving matrix. The most important factor is the gel "pore size" or the reptation "tube diameter" of the entangled polymer solution, which is considered to be the key characteristic of the matrix that controls electrophoresis. For a cross-linked polymer gel, the pore size can be tuned mainly by varying either the gel concentration (%T), defined as the monomer mass concentration used to make the gel, or by the percentage of cross-linker contained in the monomer (%C). For instance, to form cross-linked PA, acrylamide (AAm) and BIS are the two monomer components with BIS being the cross-linker, and the formed gel concentrations (%T and %C) are defined by Eqs. (6) and (7). Both factors are important in determining the microscale gel structure and therefore the matrix sieving properties for DNA separation.

$$\%\mathrm{T} = \frac{m_{\mathrm{AAm}}(\mathrm{g}) + m_{\mathrm{BIS}}(\mathrm{g})}{V_{\mathrm{sol}}(\mathrm{mL})} \times 100 \quad (6)$$

Table 2. Polymer and solvent systems with their corresponding radii of gyration

Polymer/solvent system	Dependence of $R_g{}^2$ on M (M is the molar mass of the polymer; R_g is the radius of gyration)
Rod-like	$R_g^2 \propto M^2$
Gaussian chain	$R_g^2 \propto M$
Expanded coil	$R_g^2 \propto M^{1+\varepsilon}$ (ε equals 1/5 when M is infinite)

$$\%\mathrm{C} = \frac{m_{\mathrm{BIS}}(\mathrm{g})}{m_{\mathrm{AAm}}(\mathrm{g}) + m_{\mathrm{BIS}}(\mathrm{g})} \times 100 \quad (7)$$

In Eqs. (6) and (7), m denotes the masses of each component and V_{sol} is the total solution volume. From light scattering, neutron scattering, and other measurements, the pore sizes of several kinds of cross-linked gel have been reported (Table 3). For instance, for cross-linked PA, the measured pore size by NMR is around 55 ± 15 Å at T = 9.12% and C = 5% [36].

Unfortunately, pore or tube diameters measured and/or calculated with different methods, including stationary (*i.e.*, SEM, SAXS) and dynamic methods (*i.e.*, "Ferguson plot" [37, 38]), give results that differ from each other by an order of magnitude or more. Viovy [39] suggests that this significant variation may be partly the result of the large distribution in pore/tube diameters, and the fact that different methods probe different moments of the distribution. The problem becomes even more complicated when one considers that

Table 3. Gel pore size *versus* gel type, monomer concentration, and cross-linker relative concentration, summarized from previous work as denoted in the table

Type of monomer (buffer solution)	Monomer concentration (T%)	Cross-linker concentration (C%)	Pore or tube size "*a*" (average diameter, nm)	Measurement method
Acrylamide/Bis (with TAE) [38]	10.5%	5%	42	Pore diameter estimated from Ferguson plot [37] of relative DNA mobilities[a)]
	4.6%	2%	400	
Acrylamide/Bis (with TBE) [29], [40]	10.5%	5 or 10%	38	
	4.6%	1.5%	248	
	10.5%	3%	140	
	3.5%		260	
Acrylamide/Bis [36]	16.8%	5%	3.0	NMR
	9.12 %		5.5	
	3.01 %		16.8	
Acrylamide/Bis [41]	10%	0.3%	2.2	Estimate based on the size of nanoparticles grown in the pores
		0.2%	3.4	
		0.1%	4.1	
Acrylamide/Bis (LPA covalently linked with a low percentage of cross-linker) [42]	2.5, 2.75, or 3%	4–10 mol% of the total number of moles of acrylamide monomer	460	Multiangle laser light scattering and rheometry
Acrylamide (with TBE or sequencing buffer) [43]	8%	0% (linear polymer solution)	1.4	SANS[b)]
	4%		2.4	

a) The effective median pore radius was estimated as the radius of gyration of the DNA fragment just large enough that its relative mobility is reduced to half of its free solution value.
b) SANS, small angle neutron scattering.

the mesh sizes seen by the DNA molecules are affected by the elastic deformation of the entangling network due to the interaction between the polymer fibers and DNA molecules. In addition, the sieving medium is not always homogeneous unless it is composed of artificially constructed periodic structures. However, the assumption of uniform pore or tube size is usually necessary in both simulation models and their applications to the experimental prediction, and we retain this assumption in this paper.

In our model, the movement of a DNA chain in the sieving matrix is simulated using an algorithm based generally on the idea of biased reptation [44], with an assumption of uniform tube/pore size, in which a moving chain encounters new entanglements at its leading end (head) and old entanglements get destroyed at its trailing end (tail), determined by the chain free energy. Furthermore, in our model, the electric force acts on all DNA segments instead of only on the two end segments, and the number of Kuhn steps *per* entanglement segment can change dynamically in response to the stretch of the chain by the field. In the simulation, these values are made nondimensional by dividing throughout by the average number of Kuhn steps *per* tube segment in equilibrium, which is a parameter of the model. The dynamics are based on a free energy, defined by Eq. (2), that includes both electric field and entropic elastic contributions [13]. The algorithm allows us to simulate DNA migration behavior over a wide range of field strengths, encompassing both the well-known reptation regime, as represented by region III in Fig. 1A (duplicated from ref. [45]) and the line in Fig. 1B (duplicated from ref. [3]), where $\mu \sim 1/M$ at low fields; to the oriented reptation regime, where $\mu \sim E$ as shown by region *V* in Fig. 1A and the line in Fig. 1C (duplicated from ref. [3]), which is observed at higher fields. The crossover region is also covered by our simulation, represented by a smooth transient region from reptation to oriented reptation (see the discussion in Section 2.3 and Fig. 3).

2.3 Relationships between computational and experimental parameters

2.3.1 Dimensional *versus* dimensionless electric field (*E vs.* ε)

The relationship between the reduced electric field (ε) and the real, dimensional, electric field (E) is given by the following definition (Eq. 8) involving the effective charge *per* Kuhn step ξq^{ss} and Kuhn step length b_K of ssDNA, where ξ is an effective factor to account for the fraction of charge screened by the counter ions, N_e is the average equilibrium number of Kuhn steps *per* entanglement, and k_BT is the product of the Boltzmann constant and the running temperature T.

$$\varepsilon = \frac{\xi q^{ss} N_e^{\frac{3}{2}} b_K}{k_B T} E \tag{8}$$

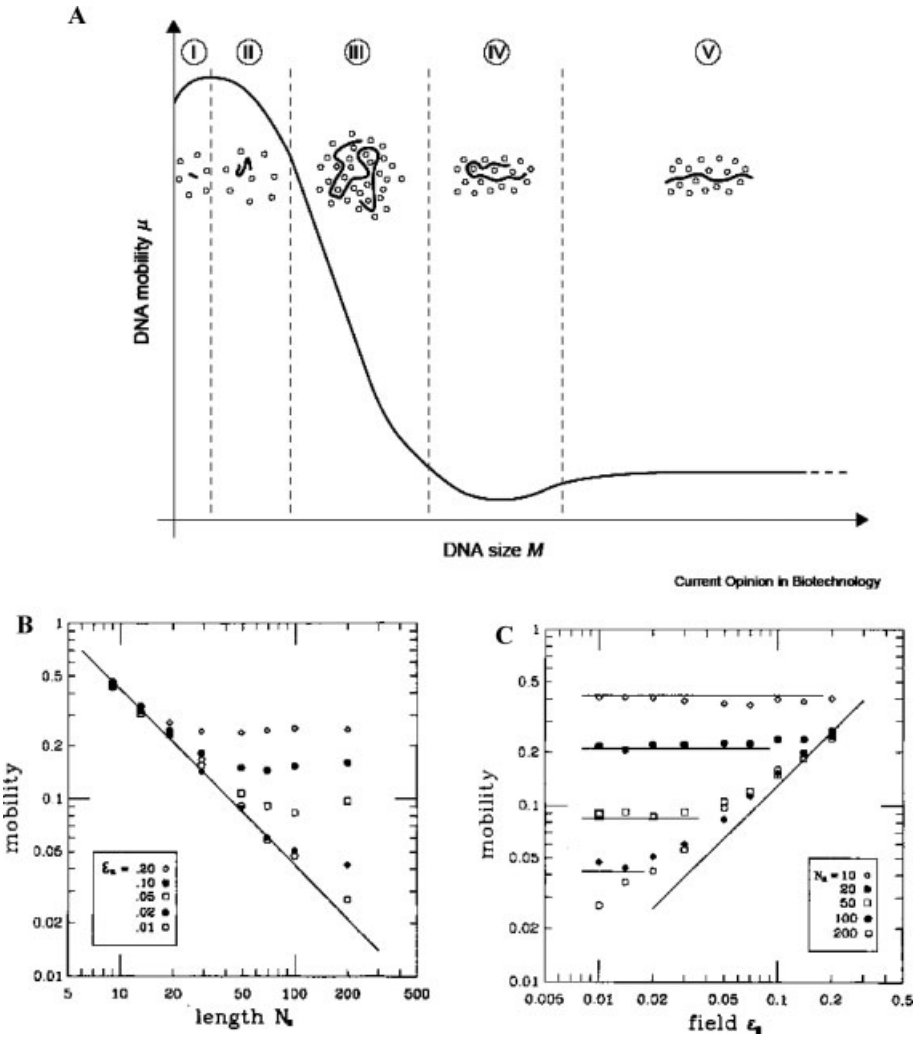

Figure 1. (A) Schematic phase diagram of the regimes of DNA separation in gels or polymer solutions by Slater *et al.* (duplicated from ref. [45]). I, Free-solution regime; II, Ogston regime; III, reptation regime; IV, intermediate regime; V, oriented reptation regime. (B), (C) The simulated reduced mobility *vs.* chain length and reduced electric field by Duke *et al.* (duplicated from ref. [3]); where $\varepsilon_a = \xi q E b_K / k_B T$; $N_a = Z(a/b_K)$. (The above equations are modified from the original format in ref. [3] for consistency with our notation.)

For dsDNA, the effective charge *per* Kuhn step (ξq^{ds}) has been measured to be approximately $-30e$, as mentioned earlier, where $e \cong 1.6 \times 10^{-19} C$ is the charge of an electron [23]. Since we know the Kuhn step length b_K^{ds} of dsDNA is around 100 nm [46], or about 300 base pairs (N_0^d), we can estimate the effective charge of ssDNA *per* Kuhn step length $b_K^{ss} \cong 5$ nm from Eqs. (9) and (10)

$$N_0^{ss} = \frac{b_k^{ss}}{L_0^{ss}} = \frac{5}{0.43} \approx 12 \text{ bases} \tag{9}$$

$$\xi q_{ss} = \frac{N_0^{ss}}{N_0^{ds}} \frac{\xi q_{ds}}{2} \approx \frac{12}{300} \cdot \frac{-30 \pm 10e}{2} = -0.6 \pm 0.2e \tag{10}$$

where L_0^{ss} is the ratio of the contour length to the number of bases for ssDNA, which is about 0.43 nm [25] and N_0^{ss} is the number of nucleotides *per* Kuhn step of ssDNA. The effective charge *per* Kuhn step of dsDNA (ξq_{ds}) is divided by 2 to account for the difference in charge density of a single strand *versus* a duplex. Therefore, assuming that the ionic screening effect, represented by ξ, is the same for both ssDNA and dsDNA, the effective charge *per* Kuhn step of ssDNA is around $-0.6e$ with an error of $0.2e$. This value is of the same order of magnitude as reported by Pluen *et al.* [47], namely $-0.4e$ *per* Kuhn step using $b_K = 8.2$ nm, and is much less than the maximum charge, $-4.2e$ *per* Kuhn step (obtained from the measured charge of $-0.6e$ per Bjerrum length (0.7 nm), and the Kuhn step length of 5 nm), above which ion condensation would occur. Pluen *et al.* used the following equation to estimate the effective charge *per* base: $\xi q = \frac{k_B T \mu_{E \to 0}}{N D_G}$; where $D_G = \frac{2 N b_0 p}{3\pi^2 \tau_2}$, and D_G is diffusion coefficient, τ_2 is the longest polymer relaxation time, N is the number of DNA bases, and $\mu_{E \to 0}$ is the vanishing-field mobility obtained by extrapolating the measured low-field mobilities to $E = 0$.

The correlation of reduced electric field with real field is calculated from Eq. (8) and shown in Fig. 2 for two sets of dimensional values. In the first, we assume that the average gel pore size (a) is 20 nm, an approximate value for a PA gel

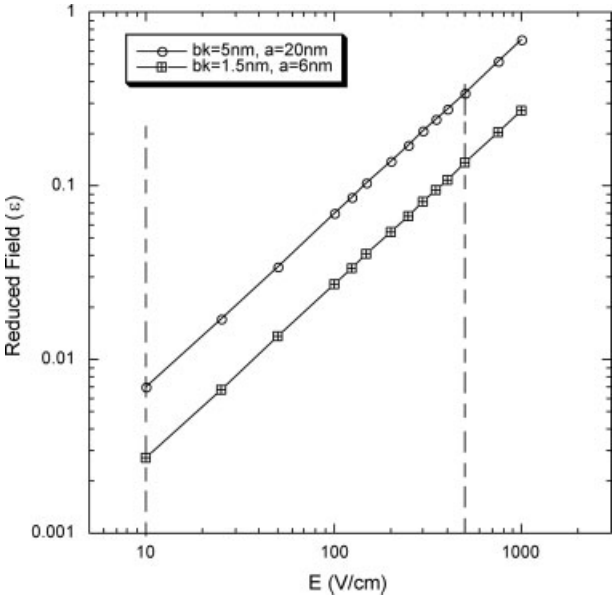

Figure 2. Dimensionless electric field *vs.* experimental electric field strength, calculated from Eq. (8) using physical properties listed in Table 1. The area between the vertical dashed lines is the range of electric field strengths usually used in either slab-gel (crosslinked polymer) or capillary (linear polymer) electrophoresis. The corresponding reduced field ranges are 0.007–0.3 for the first case (solid line with circles), and 0.003–0.1 for the second case (solid line with squares) discussed above.

of 3%T 5%C (measured by NMR), from Table 3. For ssDNA with a Kuhn step size of 5 nm ($I = 0.026$ M), the number of Kuhn steps *per* entanglement segment is $N_e = 16$ (*i.e.*, $N_e^{1/2} = a/b_K = 20/5 = 4$). We then compute $\varepsilon \approx 6.9 \times 10^{-4} \cdot E$ (V/cm) from Eq. (8) with $N_e^{1/2} = 4$, $\xi q = -0.6e$, $b_K = 5$ nm, and $T = 50$°C. In the second set of conditions, we take the gel pore size to be around 6 nm (~10%T, ~3%C PA, measured by NMR as shown in Table 3), and the Kuhn step length to be decreased to 1.5 nm, corresponding to an ionic concentration of 0.1 M; then the value of N_e also equals 16, but we obtain $\varepsilon \approx 2.07 \times 10^{-4} \cdot E$(V/cm). From these calculations, we can see that the same set of dimensionless variables can be used to describe different DNA rigidities, sieving material properties, and electric fields using different scaling factors. The temperature ($T = 50$°C) used in the calculation corresponds to the denaturing condition for ssDNA separation.

2.3.2 Dimensional *versus* dimensionless time

In our simulations, we scale time using Eq. (11) below, where τ_e is the Rouse time of an entanglement segment, *i.e.*, relaxation time of a chain segment of contour length of $N_e \times b_K$. The definition of τ_e is given in Eq. (12), where ζ is the drag coefficient *per* Kuhn step. We note that our definition of τ_e omits the prefactor of $1/6\pi$, which is merely a matter of convention. Accordingly, when N_e is a constant, the larger the Kuhn step length, the longer the real time that each dimensionless time step corresponds to. On the other hand, it is possible to keep the Kuhn step constant in the experiments, which means that the ionic strength is held fixed, and vary the pore size of the sieving medium, which will change N_e. Changing either pore size a or Kuhn step length b_K results in a change in τ_e.

$$\tilde{t} = \frac{t}{\tau_e} \tag{11}$$

$$\tau_e = \frac{\zeta b_K^2 N_e^2}{k_B T} \tag{12}$$

Our simulation results, such as the center-of-mass reduced mobility (μ^E/μ_0^E), are saved every five dimensionless time units, which is an interval denoted as t_s. Here, μ_0^E is not the free solution mobility but is the mobility of a hypothetical DNA chain in the same frictional environment as the entangled chains but with no entanglement effects (*i.e.*, in the free draining limit). Therefore, the value of μ_0^E is slightly dependent on the sieving matrix and the buffer conditions, since these affect the friction properties of the medium. Our algorithm is insensitive to time step size ($\Delta\tilde{t}$) within the range of 0.01–0.001 (see Appendix). Since τ_e is defined as the relaxation time of one entanglement segment, it can be approximated using the equation for the thermal disengagement time, Eq. (13) below, used by Viovy [39], by setting $Z = 1$, to correspond to one entanglement segment

$$\tau_{rep} \approx \frac{Z^2 a}{D_{tube}} \approx Z^3 \tau_b \tag{13}$$

where the linear diffusion constant along the tube, D_{tube}, roughly equals $k_B T/\eta a$ for a chain of length of one tube segment (a) [6]. And, τ_b is the relaxation time of a "blob" consisting of a polymer coil with radius equal to the pore size, *i.e.*, the microscopic blob relaxation time [39], which can be calculated from Eq. (14):

$$\tau_b \approx \eta a^3 / k_B T \tag{14}$$

Here, we again omit the prefactor ($1/6\pi$) from the definition of τ_e. In the above equation, η is the solvent viscosity and can be taken as the viscosity of water at 50°C (under denaturing conditions), namely 0.50 cP. Taking the pore size or tube diameter to be $a = 20$ nm, Eq. (14) then yields a disengagement time of ~1 μs for a blob size of 20 nm, which is the relaxation time of an entanglement segment. This approximation to τ_e will be evaluated in our later discussion.

2.3.3 Dimensionless *versus* dimensional mobility

Electrophoretic mobility is defined as the migration velocity divided by the electric field. Our simulation program records the velocity of the molecular mass center every $5/\Delta\tilde{t}$ time steps (*e.g.* each $\tilde{t}_s = 5$) and then averages over the recorded

points. As described in our earlier paper, the simulated mobility can be written as

$$\tilde{\mu} = \frac{\mu^E}{\mu_0^E} \quad \text{and} \quad \mu_0^E = \frac{q\xi}{\zeta} \tag{15}$$

where μ_0^E was defined earlier as the mobility of a DNA chain that is not constrained by entanglements with the matrix and ζ is the drag coefficient *per* Kuhn step. The simulation starts with the generation of one chain with randomly formed entanglement points. The effect of the initial chain configuration on the average value of mobility can be ignored since our results are averaged over a time period hundreds of times longer than the full chain relaxation time. We confirmed this by leaving out the initial portion of a run, and found that it had no effect on the resulting average.

2.3.3.1 Reduced mobility *versus* reduced field

The final results are shown in Fig. 3 (the symbols) for chains of various lengths at different dimensionless electric fields. Our simulation results more smoothly resemble experimental results than do scaling-only theories (see Figs. 3 and 7 below), since our simulations give a smooth crossover transition from the low-field reptation regime to the biased reptation regime, and fit well with the theory at a high field as $\mu \propto \varepsilon$. All lines in the plot are from the "interpolation equation", which will be discussed below. The error bars are standard errors calculated based on mobilities of all sampling points, the number of which varies from run-to-run within the range of 10^5–10^6. The model tends to fail when $Z < 8$ (not shown in the figure), where the reduced mobility computed for shorter chains is smaller than the mobility value for $Z = 8$. We attribute the failure of chain sizes smaller than $Z = 8$ to their weak entanglement with the network, because for $Z < 8$ the radius of gyration (Table 4) becomes comparable to the tube or pore size (20 nm).

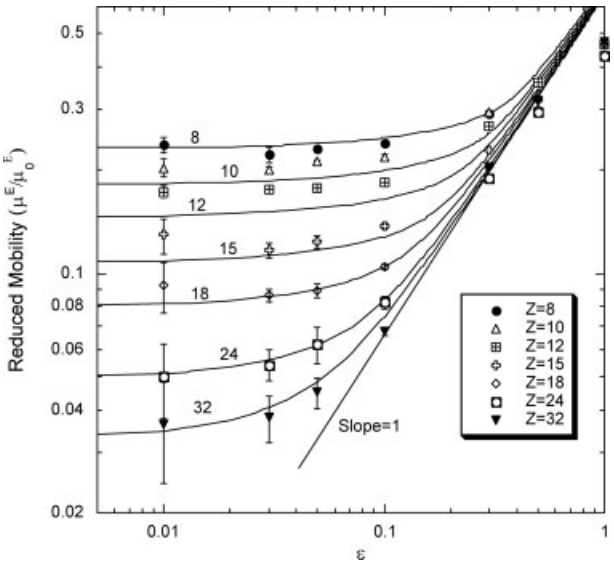

Figure 3. Symbols: reduced center-of-mass mobility *vs.* reduced field (as defined in part 1), for various chain lengths Z with $N_e = 16$ and $\Delta\tilde{t} = 0.01$. Z is the average number of entanglements of one DNA chain with the network and N_e is the average equilibrium number of Kuhn steps between entanglements, *e.g.*, within one tube segment. Curves: asymptotic fittings with the interpolation equation, as defined in Eq. (18), for reduced mobility simulated under various reduced electric fields and with different entanglement numbers.

Table 4. The radius of gyration of ssDNA molecules as a function of the number of entanglements in a gel of pore size 20 nm with $b_K = 5$ nm. ($N = Z\,\frac{N_e b_K}{b_0}$, $b_0 = 0.43$ nm)

Entanglement number (Z)	Number of bases ($N_e = 16$, $b_K = 5$ nm)	Radius of gyration (R_g) (nm)
8	1488	23.07
10	1860	25.79
12	2233	28.26
15	2790	31.59
18	3349	34.61
24	4465	39.96
32	5953	46.14

2.3.3.2 Reduced mobility *versus* entanglement number

Theoretically, the mobility at low electric field is proportional to the reciprocal of DNA chain size N, which is represented by the number of entanglements *per* chain (Z) in our model when N_e is a constant. Hence, we may expect a plot of reduced mobility *versus* the entanglement number to follow a power law scaling $\tilde{\mu} \propto Z^{-1}$ when $\varepsilon << 1$. As plotted in Fig. 4, $\frac{\mu^E}{\mu_0^E} \propto Z^{-1.68}$ is observed for chains with $Z > 10$ at low reduced field ($\varepsilon = 0.01$). Therefore, an asymptotic equation, given in Eq. (17), was obtained by fitting the reduced mobility values for $Z > 10$. The slopes of power-law fits for computed results and for experimental data are listed in Table 5 for comparison. As we can see, all power-law equations deviate from the theoretical prediction: fits to the simulation results always give a slope steeper than -1 while fits to the experimental data always have an index less than -1. The deviation from a slope of -1 in our simulations is believed to be a result of nonlinear spring effects when N_e is relatively small, so that the simulated mobilities do not agree with the scaling law ($\mu \propto N^{-1}$), which is derived based on the assumption of ideal Gaussian chains.

A possible reason for the deviation of experimental slopes from the theoretical value (-1) is that the low field limiting case may not be fully realized in the experiments since for large DNA molecules very low fields are required to achieve this limit (see Eq. 16; [8]), which is not realistic due to the extremely slow migration rate. Analytically, we can see how a slope less steeper than -1 will be obtained from Eq.

Table 5. Power-law fits to log–log plots of mobility *vs.* ssDNA size for simulations and experiments

	Simulation results		Experimental results[a)]		
	Simulation results at $\varepsilon = 0.01$ ($N_e = 16$)	Simulation results at low field ($N_e = 100$) [13]	HEC 0.3%	HEC 0.5%	HEC 0.7%
Slope	−1.68	−1.32	−0.332	−0.443	−0.672

a) The slopes of experimental results were obtained from data of Todorov and Morris [48], for ssDNA electrophoresis in HEC solutions of various concentrations with 0.5 × TBE and 4 M urea.

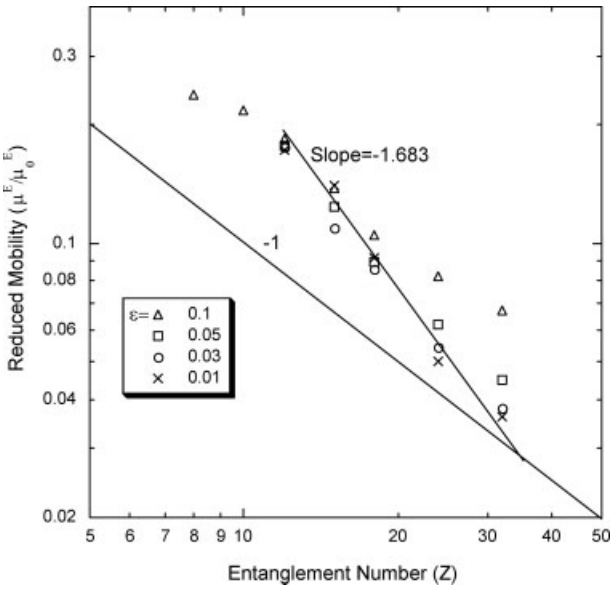

Figure 4. Reduced mobility *vs.* number of entanglements *per* chain at a low dimensionless electric field. A power law slope of –1 corresponds to DNA migrating *via* the reptation mode (*e.g.*, $\mu \propto \frac{1}{N}$), independent of the field strength at a low field (Eq. 16). For clarity, only the averaged center-of-mass mobilities without error bars are plotted.

(16) when N is large, and ε is not comparably small (*e.g.* $\varepsilon > 1/N$). There is also a relatively large discrepancy between the power-law index that fits our simulation results and the index that fits to the experimental data for 0.7% hydroxyethylcellulose (HEC), although the estimated tube diameter of 0.7% HEC (19 nm) [48] is very close to the pore size (20 nm) assumed in our simulations. This may be due to the pore size distribution in the real gel, and thus nonconstant N_e, which is not considered in the simulation.

$$\frac{\mu}{\mu_0} = [(3N)^{-2} + (2\varepsilon/5)^2]^{1/2} \tag{16}$$

An analytical asymptotic formula for the mobility (Eq. 17) is derived by a fit to our simulation data, and will prove to be useful in later discussion (see below). This equation is obtained using an approach similar to that used by Graham and Larson [13]. That is, simulation results at $\varepsilon = 0.01$ are fitted with an empirical functional form expected from reptation theory in the asymptotic limit of low field. The calculated reduced mobility from this asymptotic equation fits the simulation results well when $Z > 10$ for $N_e = 16$ (Fig. 5). The deviation at small molecular sizes ($Z < 10$) may indicate a transition away from reptation, which is not encompassed in our model.

$$\tilde{\mu}^E_{low} = \exp(-0.18Z) + \frac{1}{Z}[1 - \exp(-0.0016Z^{2.7})] \tag{17}$$

(Asymptotic equation)

In order to further interpolate our simulation results from the low-field plateau regime ($\tilde{\mu} \propto \varepsilon^0$) to the high-field regime ($\tilde{\mu} \propto \varepsilon^\alpha$, and $\alpha = 1$ with BRF theory), we use Eq. (18) (which we call the interpolation equation), which describes the reduced mobility as a function of both the reduced field and the entanglement number across the whole set of simulation results for $N_e = 16$ and yields curves fitting the simulation results well in Fig. 3. This equation also provides us a convenient way to compare our simulations with experiments, as we will discuss in Section 2.4.

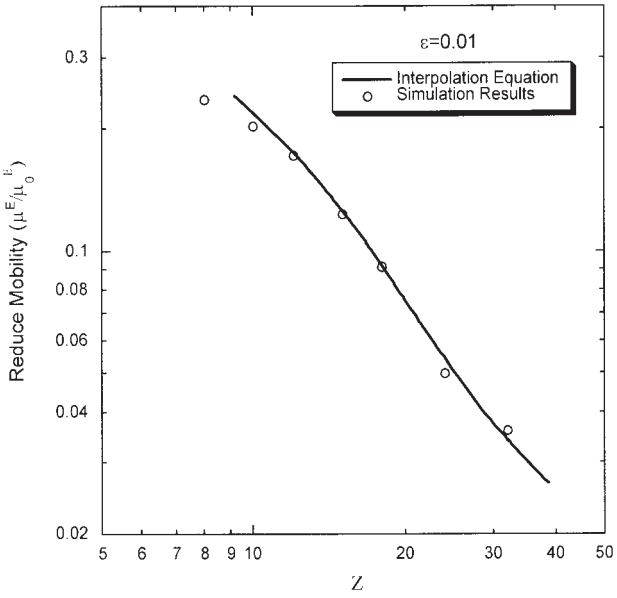

Figure 5. Symbols: simulated reduced mobilities at low field ($\varepsilon = 0.01$); curve: the fit by Eq. (17).

$$\frac{\mu^E}{\mu_0^E} = \frac{m\varepsilon}{2} + \frac{\tilde{\mu}_{low}^E}{2} + 0.3\sqrt{am + m^2\varepsilon^2 - 2m\tilde{\mu}_{low}^E + \tilde{\mu}_{low}^{E\ 2}} \quad \left(m = 0.8, a = \frac{0.3}{Z^{1.5}}\right) \tag{18}$$

(Interpolation equation)

Equations (17) and (18) are chosen primarily for mathematical convenience to interpolate between the asymptotic limits of the model. However, there is also a physical basis for the asymptotic behavior of both equations. Equation (18) is a hyperbola, which scales as ε^0 at low ε and as ε^1 at high ε. The physical basis for these asymptotic regimes is reptation without orientation or reptation with orientation, respectively. Equation (17) captures the low-field limit of the BRF model, in which the low field mobility scales as $1/Z$. Again, this asymptote has a physical explanation and arises the electric force acting on the equilibrium chain configuration balanced by the chain drag. However, the scaling of mobility with Z for shorter chains is not currently understood in terms of simple physical arguments.

2.3.3.3 Reduced mobility *versus* N_e

In the previous work [13], computations were done with $N_e = 100$ to simulate dsDNA mobility in an agarose gel, near the limit of $N_e \to \infty$. In this paper, we take $N_e = 16$, to account for differences in both the properties of DNA chains (single strand *vs.* double strand) and those of the network (agarose *vs.* highly entangled polymer solution or gel). It is worthwhile comparing the results for $N_e = 16$ and $N_e = 100$ to predict how the mobility depends on the number of Kuhn steps *per* tube segment when varying either the Kuhn step length or the tube diameter. In this way, we will be able to apply our model over a wider range of experimental conditions, such as different buffer ionic strengths (varying b_K) or gel concentrations (varying a).

As shown in Fig. 6A, the dependence of reduced mobility on electric field for $N_e = 16$ is similar to that with $N_e = 100$, except for a systematic reduction in μ^E/μ_0^E for $N_e = 100$ relative to $N_e = 16$. Furthermore, we have the reduced mobilities computed for a series of N_e for chains with fixed entanglement number ($Z = 15$). The relationship between $\tilde{\mu}$ and N_e is clearer when we plot the reduced mobility *versus* different N_e with a fixed Z and ε, as shown in Fig. 6B. A sharp decrease in the reduced mobility occurs with an increase in the number of Kuhn steps *per* tube segment from $N_e = 2$–10, and a plateau is reached when $\sqrt{N_e} > 20$. The trend can be fitted with $\frac{\mu^E}{\mu_0^E} = m_1 + m_2 \exp(-m_3 I^{0.5}) + N_e^{-m_4/2}$, where $m_1 = 0.09$, $m_2 = 0.14$, $m_3 = 0.32$, and $m_4 = 3.7$.

As defined, N_e is a function of both ssDNA Kuhn step length (b_K) and the pore size (a). Therefore, a change in either of these parameters will result in a different value of N_e. Experimentally, such a change could be caused by changes in gel type and concentration, or buffer type and/or

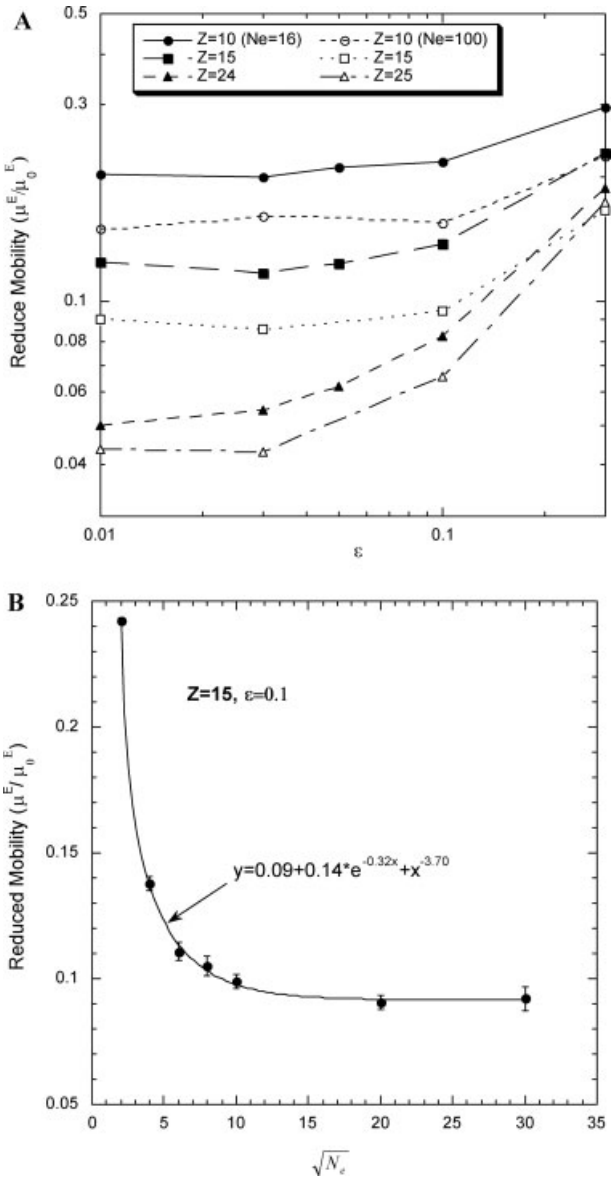

Figure 6. Dependence of simulated reduced mobility on N_e. (A) Field dependence of dimensionless mobility computed for $Z = 10$, 15, 24 (25) using N_e $\sqrt{N_e} = 4$ (closed symbols) or $\sqrt{N_e} = 10$ (open symbols). (B) Reduced mobility as a function of the square root of the number of Kuhn steps *per* entanglement ($\sqrt{N_e}$) with fixed entanglement number ($Z = 15$) at a reduced field of $\varepsilon = 0.1$.

concentration. Tinland *et al.* [21] have systematically studied the relationship between ssDNA persistence length (p) and ionic strength (I) of TBE buffer solution. A power-law decrease in b_K with I (Fig. 2 of ref. [21]), $b_K \propto I^{-0.5}$, has been sketched for the experimental observations. Because N_e is proportional to b_K^{-2}, we estimate $N_e \propto I$ and then have $\frac{\mu^E}{\mu_0^E} = m_1 + m_2 \exp(-m_3 I^{0.5}) + I^{-1.85}$ derived from the above fitted equation. Such a functional form with the assumption

of uniform constant pore size could be compared to measurements of ssDNA that is long enough to be well entangled with the network, in an artificial periodic structure [49], with buffer solutions of different ionic strengths.

Note in Fig. 6B, that the mobility ratio $\mu^E/\mu_0{}^E$ increases rapidly at fixed Z and ε as N_e decreases. When N_e shrinks to unity or smaller, our model fails, since the model assumes that the DNA Kuhn step length is much smaller than the pore size, *i.e.*, $N_e >> 1$. Thus, the steep increase in $\mu^E/\mu_0{}^E$ as N_e approaches unity may not be quantitatively accurate. Theoretically, N_e determines the degree of chain stretch when the nonlinear spring force (finite extensibility) begins to influence the mobility. For high N_e, the chain can accumulate a large amount of stretch without the nonlinear spring effect being seen. Thus, the nonlinear spring effects are not seen for large N_e and so the mobility becomes independent of N_e, which results in the plateau at higher N_e ($N_e > 20$).

2.3.4 Dimensionless *versus* dimensional migration distance and variance

In real electrophoresis, the migration distance must be made large enough to resolve DNA bands of different sizes. A primary goal of our simulations is to provide estimates of the required separation distance needed for resolution. To achieve this, we first need to assign a dimensional value corresponding to the scaled time. We also need to convert the scaled time $\tilde{t}$ into the dimensionless migration distance ($\tilde{l}$) using Eq. (19) involving the average dimensionless mobility of the DNA chain and the reduced field. The real migration distance (l) can be retrieved from this dimensionless value using Eq. (20) once we know the values of N_e and b_K [13].

$$\tilde{l} = \tilde{\upsilon} \cdot \tilde{t} = \frac{\mu^E}{\mu_0^E} \varepsilon \cdot \tilde{t} \tag{19}$$

$$\tilde{l} = \frac{l}{\sqrt{N_e} b_K} \tag{20}$$

The intensity distribution in a DNA band, characterized by the peak width, is a key factor in determining the resolution. To calculate the width of electrophoretic bands, and therefore the resolution of one band from another, we need to know the SD (σ) or variance (σ^2) of mobility, so that the peak shape can be calculated by assuming that the peaks are Gaussian. The SD of short-time mobilities (σ_s) is computed from the distribution of mobility values (Eq. 21), each of them an average over a fixed short time period ($\tilde{t}_s$). One can use the SD of the short-time mobility (σ_s) to predict the long-time SD (σ_t) as long as $\tilde{t}_s$ is longer than the autocorrelation time for mobility fluctuations, which will be discussed in Appendix. By applying the central limit theorem, we can calculate the SD for mobilities averaged over any time period *via* Eq. (22).

$$\sigma_s^2 = \frac{\sum_{i=1}^{N} \mu_i^{E\,2}}{N-1} - \frac{\left(\sum_{i=1}^{N} \mu_i^E\right)^2}{N(N-1)} \tag{21}$$

$$\sigma_t = \sigma_s \sqrt{\frac{t}{t_s}} \tag{22}$$

2.4 Comparison with experiments

To compare our simulation results to experiments, we use two methods to convert our simulated reduced mobilities to dimensional "real" values. In the first method, we take the value of μ_0^E to be a constant by neglecting any possible changes caused by differences in the sieving matrix. Instead of using the definition (Eq. 15) to calculate μ_0^E, we use the mobility of short DNA oligomers in a PA gel (4%T, 3%C) as an approximation, yielding $\mu_0^E \sim 2 \times 10^{-4}$ cm^{2}V^{-1}s^{-1} [33]. Then, we calculate the real migration mobility μ^E using $\mu^E = \tilde{\mu}\mu_0^E$ from the simulated reduced mobility $\tilde{\mu}$. For instance, the simulated reduced mobility $\tilde{\mu}$ is ~0.18 for $Z = 12$ at $\varepsilon = 0.1$, as shown in Fig. 4. The real mobility for a chain with 12 entanglements at a reduced field $\varepsilon = 0.1$ is then calculated to be $\mu^E \approx 0.18 \times 2 \times 10^{-4}$ cm^{2}V^{-1}s^{-1} = 3.6×10^{-5} cm^{2}V^{-1}s^{-1}. We also have $\tau_e = 1$ μs as estimated in Section 2.3.2 for one DNA segment within a pore/blob size of 20 nm. Therefore, a dimensionless time $\tilde{t} = 6 \times 10^6$ corresponds to a real time of 6 s. The dimensionless migration distance is then calculated to be 1.08×10^5 from Eq. (19) with the known $\tilde{\mu}$, ε and $\tilde{t}$. Thus, the corresponding real distance is determined to be 2.16 mm *via* Eq. (20) $N_e = 16$ and $b_K = 5$, as used in the computations. Note here that the consistency of the estimation of real migration distance and real time can be checked by setting the value of either real distance or real time equal to that of the experiment, and then comparing the predicted value of the other to the experimental value.

In addition, we have calculated the corresponding DNA size to be approximately 2.2 k base pairs for a chain with 12 entanglements (Table 4), for $N_e = 16$ and $b_K = 5$ nm. The mobility of ssDNA-sized 2038 base pairs is about 8.02×10^{-5} cm^{2}V^{-1}s^{-1}, as measured by Todorov and Morris [48], in a 0.7% HEC polymer solution (estimated tube diameter 19 nm). Therefore, for an ssDNA chain of 2.2 k base pairs to migrate a distance of 2.16 mm under an electric field of 150 V/cm (corresponding to $\varepsilon = 0.1$), the experimental running time is calculated to be about 18 s ($t = \frac{l}{\mu E}$), which is roughly comparable to the value (6 s) derived from the scaled time by assuming that the relaxation time of one entanglement segment equals 1 μs. The difference is presumably due to the approximations we have made for the properties of ssDNA and the sieving matrices, especially the blob relaxation time, which is estimated using the viscosity of water in calculation with Eq. (14). The comparison indicates that the actual relaxation time of one entanglement segment might be longer than 1 μs for a pore/blob size of 20 nm. An alter-

native estimation for the relaxation time comes from the longest relaxation time (τ_2) measured for an ssDNA molecule of 2961 base pairs, namely 0.06 s in a PA gel of 4%T and 3%C, by Pluen *et al.* [47]. Since the longest relaxation time is proportional to N^3 ($\tau_2 \propto E^0 N^{3.0} T^{1.2}$), where N is the size of DNA chain, the relaxation time (τ_e) for one DNA of length sufficient to fill one tube segment, *i.e.*, 180 base pairs (corresponding to $b_K = 5$ nm and $a = 20$ nm) works out to be about $\tau_e = 13$ μs. Therefore, a more realistic estimation might be that the relaxation time τ_e is in the range of 1∼10 μs. In Section 2.5, we will use the value $\tau_e = 5$ μs to calculate the peak width, which gives a very good agreement with experimental results.

The second way to compare our simulation results to experiments is by using the interpolation equation derived above (Eq. 18) to obtain reduced mobilities of various DNA sizes using different sets of parameters, corresponding to various experimental conditions (*i.e.*, various values of E, a, and I). Some of the properties, including the Kuhn step length and the pore size, assumed in the above calculations, need to be modified, as listed in Table 6, in order to match the values used in the experiments. The reduced values are converted to real values by setting μ_0^E to the mobility of the smallest ssDNA chain in the experiment, assuming there are no entanglement effects on the smallest chain. The calculated results (curves) are then compared to the experimental data of Todorov and Morris (symbols in Fig. 7). For ssDNA with fewer than 1000 base pairs, the predictions of our interpolation equation match the experimental data well, while there is a relatively large deviation for larger DNA chains ($N >$1000 base pairs), indicating the need for further refinements of the theory. One possible cause of the deviation in mobility values for longer ssDNA chains is the missing constraint-release effect in our simulation model, which has a greater effect on longer chains than on shorter ones. Therefore, the interpolation equation, which is based on the simulation results, gives better prediction for the mobility of shorter chains than for longer chains.

On the other hand, we have noticed that although the simulated reduced mobilities of chains with fewer than ten entanglements deviate somewhat from our asymptotic and interpolation equations, we are able to use these equations to match many (but not all) experimental results for relatively small ssDNA chains, as shown in Fig. 7. A possible reason for deviations is the imprecise value of estimated/measured pore size or tube diameter from the experiments. As shown in Table 3, the pore size of a PA gel with 10.5%T, 5%C, estimated from a Ferguson plot, is 38 nm while the same kind of gel at modestly lower crosslinker concentration (10%T, 3%C) has a pore size estimated as 4 nm by measuring the size of nanoparticles grown in the pores. Rousseau *et al.* [33] proposed a very effective way for estimating pore size by plotting 3 μM/μ_0 *versus* M, where M is the DNA molecular weight in units of bases. Using the reptation theory, Rousseau *et al.* determined that the intercept on the y-axis corresponds to the size of the DNA, M_a, which just fits into one pore (a).

Table 6. Amended parameter values for ssDNA used to convert dimensionless into dimensional values

	b_K(nm)	(nm)	N_e	($cm^2V^{-1}s^{-1}$)	ε
Original (simulation)	5	20	16.00	N/A	0.01, 0.03, 0.05, 0.1, 0.3, 0.5, 1
Amended (Fig. 7)	4	19	22.56	2.73×10^{-4}	0.018–1

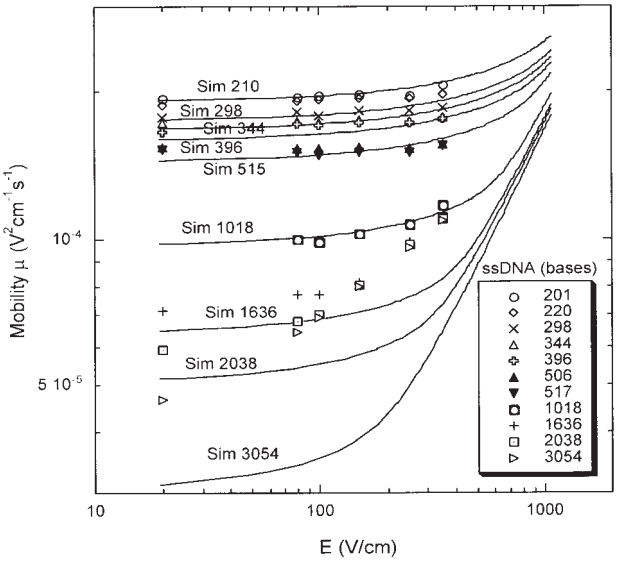

Figure 7. Prediction of mobility *vs.* electric field (lines) by the interpolation equation (Eq. 18) compared to the experimental results (symbols) replotted from Fig. 5B of ref. [48]. The size of ssDNA denoted in the legend is in units of bases. Reduced mobilities are first calculated from the interpolation equation with modified values: $a = 19$ nm, $b_K = 4$ nm, $\xi q = 0.6e$ and then converted into mobility in the same units as the experimental data by using the scaling factor $\mu_0^E = 2.73 \times 10^{-4}$ $cm^2V^{-1}s^{-1}$, which is obtained by dividing the experimental mobility (μ^E) of ssDNA (201 b) by the reduced mobility ($\tilde{\mu}$) for the same size chain.

This scaling method for the pore size can be conveniently used to estimate N_e with $N_e = \dfrac{a^2}{b_K^2} = \dfrac{M_a}{N_0}$, where N_0 is the number of bases *per* Kuhn step. With this equation, we can use the measured ssDNA mobility curve to extract a value for N_e by plotting 3 μM/μ_0 *versus* M, and avoid any possible error induced by the imprecise pore or tube size measured with different methods [39].

2.5 Peak width and resolution

2.5.1 Peak width

After obtaining the theoretical dimensionless SD of the mobility as described in Section 2.3, we can use Eq. (23) to cal-

culate the dimensionless theoretical peak width ($\widetilde{hw}$), which can be converted into a corresponding experimental value using the same scaling factor as in Eq. (20) (see Eq. 24). In experiments, the peak width is determined by the dispersion (diffusion under external electric field) along with several other factors. As shown in Eq. (25), the total variance in mobility contains contributions from dispersion ($\sigma^2_{\rm dis}$), which is the variance in mobility caused by both simple Brownian diffusion as well as fluctuations in the polymer response to the electric field, from the temperature gradient in the migration direction ($\sigma^2_{\Delta T}$), from DNA adsorption ($\sigma^2_{\rm ads}$) to the network and inner wall surface, from the initial injected bandwidth ($\sigma^2_{\rm inj}$), and from the width of the detection region ($\sigma^2_{\rm det}$). Our simulations account only for $\sigma^2_{\rm dis}$, which is the minimum band broadening obtained under ideal electrophoresis conditions (no temperature gradient, no heterogeneity in microstructure, no adsorption, zero injection width, *etc.*). Hence, our predictions are only semiquantitative and need to be combined with estimates for other effects to give more quantitative predictions in the future.

$$\widetilde{hw} = 2\sigma_{\rm l}\sqrt{2\ln 2} = 2\sqrt{2\ln 2}\sigma_{\rm t}\varepsilon \tag{23}$$

$$hw = \widetilde{hw}\sqrt{N_{\rm e}}b_{\rm K} \tag{24}$$

$$\sigma^2_{\rm tot} = \sigma^2_{\rm dis} + \sigma^2_{\Delta T} + \sigma^2_{\rm ads} + \sigma^2_{\rm inj} + \sigma^2_{\rm det} \tag{25}$$

Figure 8 shows the dimensionless peak width calculated for DNA chains with $Z = 8$–50 entanglements *per* chain. Using the value $N_{\rm e} = 16$ and a Kuhn step length of 5 nm that are appropriate for most of the running conditions in ssDNA electrophoresis, the real DNA sizes for these chains are in the range from ~1500 base pairs ($Z = 8$) to ~9000 base pairs ($Z = 50$), which have not been as well investigated experimentally as have chains smaller than 1000 base pairs. Nevertheless, we find experimentally that there is a decrease in peak width for increased DNA length, as is predicted by the simulation when the entanglement number exceeds a threshold (Z^*), that appears to depend on the electric field. For low electric fields ($\varepsilon < 0.1$), the calculated peak width does not change significantly with the electric field intensity until $Z > 24$ (*i.e.*, the data in Fig. 8 collapse together for $\varepsilon < 0.1$ until Z reaches around 24), which is similar to the observed slight decrease in the dispersion coefficient with increased ssDNA size in a cross-linked PA gel (6, 9, or 12%*T*), as reported by Lo and Ugaz [50] (Fig. 4 in their paper). The predicted change of peak width with entanglement number follows a power law with a slope of -1 in the linear region (Fig. 8). In our simulations, the peak width is only due to dispersion, so that $hw = \sqrt{D^{\rm E}t} \propto N^{-1}$ where $D^{\rm E}$ is the dispersion coefficient, and therefore $D^{\rm E} \propto Z^{-2}$. This scaling is the same as the prediction by Slater *et al.* [45], for the diffusion coefficient when $N < \varepsilon'^{-2/3}$ based on the BRF model, where N in their work is the same as Z in ours, and $\varepsilon' = \dfrac{\eta a^2 \mu_0 E}{k_{\rm B}T}$ in their work. The

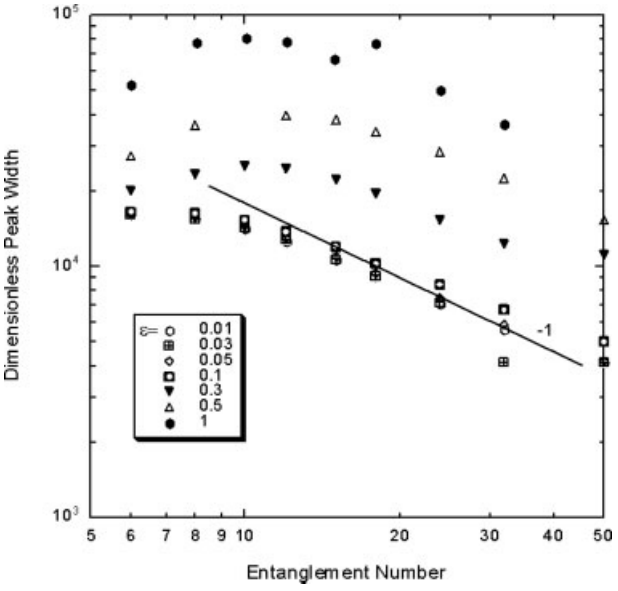

Figure 8. Dimensionless peak width (spatial) for DNA chains migrating under various reduced fields (ε) for a constant dimensionless migration time: $\tilde{t} = 6 \times 10^8$. The line in the plot has a slope of -1, which is consistent with the prediction from reptation theory.

critical entanglement number, defined as the value of Z above which the relationship of $D^{\rm E} \propto Z^{-2}$ becomes invalid is then calculated from the condition $N < \varepsilon'^{-2/3}$ to be ~29 when $\varepsilon = 0.05$ or ~18 when $\varepsilon = 0.1$, under the conditions we simulated, *i.e.* $a = 20$ nm, $\mu_0 = 2 \times 10^{-4}$ cm^{2}V^{-1}s^{-1}, $\varepsilon = 6.9 \times 10^{-4} E$ (V/cm) and $T = 50$°C. The estimated critical values of entanglement number are consistent with the trend of dimensionless peak width change with Z, as shown in Fig. 8. At higher fields, Fig. 8 shows that the band broadening is predicted by our model to be greater than can be accounted for by simple molecular diffusion, which can be represented by the dimensionless bandwidth under vanishing field (*e.g.* $\varepsilon \leq 0.05$), and hence field-induced fluctuations in DNA mobility must also contribute to the bandwidth.

2.5.2 Gaussian peaks

To determine electrophoretic resolution, we reconstruct multipeak plots (each peak standing for one DNA band) by assuming all peaks are Gaussian. As an example, a set of DNA bands at a constant migration time is plotted in Figs. 9A and B for two values of reduced field. This plot is analogous to an image taken for a slab-gel electrophoresis experiment. The center of each peak in Fig. 9 is determined by the averaged reduced mobility and the preassigned dimensionless time, and the peak width is calculated in the same way as in Fig. 8.

In CE experiments, the peak width and peak spacing are obtained at the "finish line", and given in terms of time at a constant migration distance. To compare our simulated peak

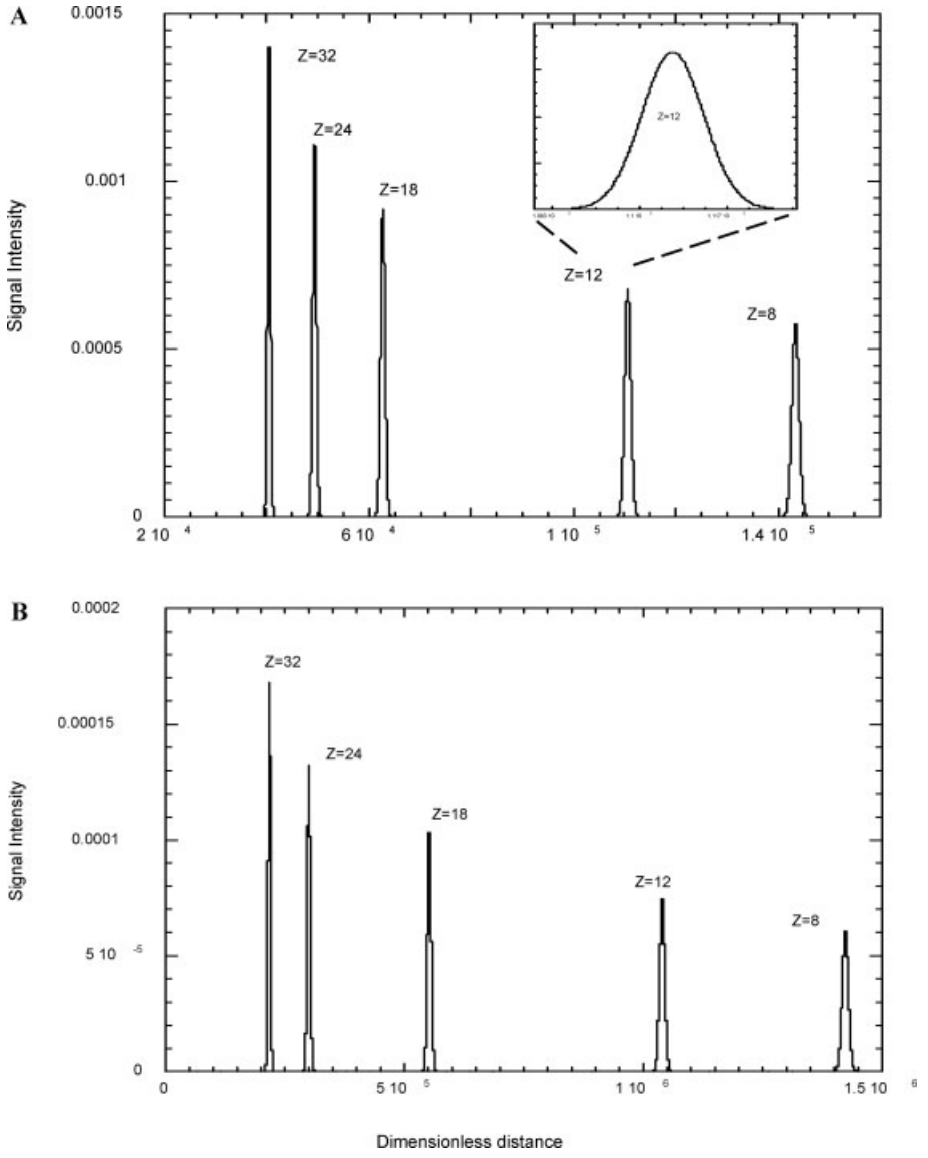

Figure 9. (A) Reconstructed Gaussian peaks for reduced field $\varepsilon = 0.1$ (corresponding to ~150 V/cm in a typical real experiment) where each peak stands for the band position and distribution (in terms of distance) at the time $\tilde{t} = 6 \times 10^6$ (~6 s in a typical real experiment with $\tau_e = 1$ μs). The peak for $Z = 12$ has been enlarged in an inset plot to show the Gaussian shape. (B) Reconstructed Gaussian peaks for reduced field $\varepsilon = 0.01$ and $\tilde{t} = 6 \times 10^8$. Parameters used in both (A) and (B) are $N_e^{1/2} = 4$ and $\Delta\tilde{t} = 0.01$. The *x*-axis is the dimensionless value of migration distance ($\tilde{l}$), which can be readily converted into real distance using $l(\text{mm}) = 2 \times 10^{-5}\tilde{l}$, roughly corresponding to 2.8 cm for the first band in (B). The value of the *y*-axis is obtained using a Gaussian distribution with integrated probability normalized to unity.

width and resolution to such experimental results, we need to change our calculation from constant time to constant distance. In our previous discussion, we stated that the SD, which we used to predict the width of the peaks, is calculated from simulated mobilities averaged over small fixed time intervals. To rebuild the distribution over time rather than distance, we assume that the peak width is small enough compared to the migration distance that we can take the relative spatial distribution at the moment when the center of the peak passes the detection point as the relative temporal distribution. That is, the temporal distribution, when normalized by the mean time, is simply taken as the spatial distribution normalized by the mean distance, where this mean distance is the position of the finish line. In this way, we obtain the plot of Gaussian peaks in terms of time as shown in Fig. 10 for a reduced field $\varepsilon = 0.1$.

The rebuilt peaks are narrow, consistent with our assumption. For instance, the peak width is about 10^6 for $Z = 12$ after migrating 9.75×10^8, both in units of dimensionless time. The dimensionless time can then be converted to real time using $\tau_e = 5$ μs, giving a real width of 5 s. The real-time width of 5 s corresponds to a band with spatial width of ~3.7 mm, for a hypothetic DNA chain of size 2233 base pairs (Table 4) after migrating ~80 min under a field of 150 V/cm. This bandwidth is identical to the value of bandwidth calculated from the longitudinal dispersion coefficient (3×10^{-7} cm^2/s) for a ssDNA chain of size 2961 base pairs in experiments of Pluen *et al.* [47] under an electric field of 105 V/cm in a 4%T, 3%C PA gel. This similarity in predicted *versus* measured bandwidths verifies our new estimate for τ_e as well as the prediction for the peak width based on the simulations.

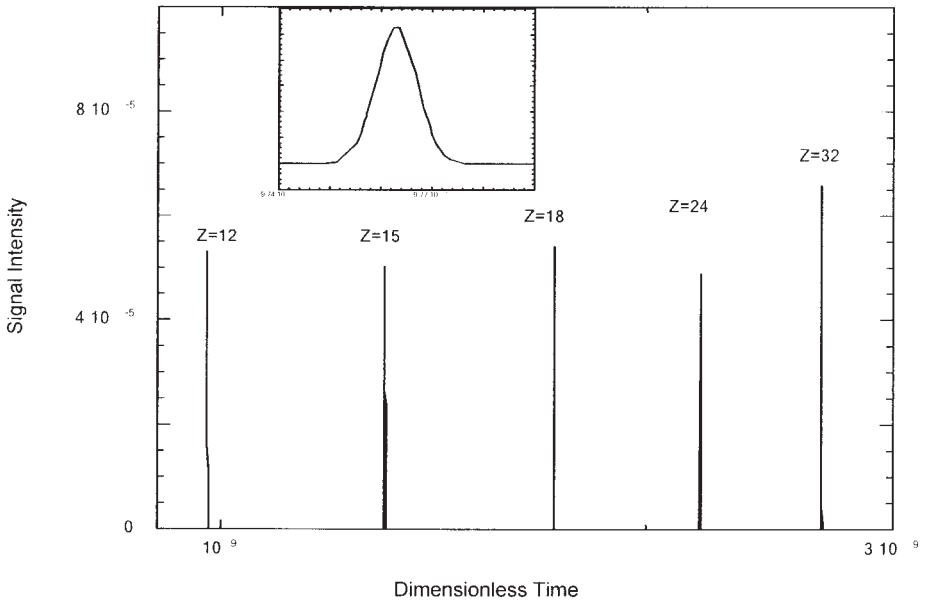

Figure 10. Reconstructed Gaussian peaks with a constant migration distance $\tilde{l} = 1.8 \times 10^7$ (equivalent to 36 cm when $N_e = 16$ and $b_K = 5$ nm) at reduced field $\varepsilon = 0.1$ (corresponding to ~150 V/cm in a typical experiment). The peak width and spacing are in terms of time while the signal intensity is calculated based on a normalized Gaussian distribution.

Furthermore, the resolving power (*e.g.*, resolution) for two different DNA molecular lengths of interest can be calculated using Eq. (26), which involves both the center-to-center distances (l_1, l_2) and the peak widths at half height (hw_1 and hw_2) of the two theoretical bands.

$$R_s = \frac{l_2 - l_1}{hw_1 - hw_2} \tag{26}$$

With our simulated results shown in Fig. 9A, the resolutions between two neighboring peaks with various entanglement numbers, are $R_s = 12.8$ ($Z = 8$, 12), 23.4 ($Z = 12$, 18), 8.4 ($Z = 18$, 24), and 6.9 ($Z = 24$, 32) with $\varepsilon = 0.1$ and $\tilde{t} = 6 \times 10^6$. And $Z = 12$ with $\varepsilon = 0.1$ and $\tilde{t} = 6 \times 10^6$ corresponds to a DNA of size 2232 b when $a = 20$ nm, $b_K = 5$ nm for chains running under an ideal condition (no injection bandwidth, no temperature gradient and so on) with a field of ~150 V/cm running for ~30 s. Resolution *per* entanglement here is calculated to be 3.2, 3.9, 1.4, 0.86 for pairs of neighboring peaks from ($Z = 8$, 12) to ($Z = 24$, 32). The resolution *per* entanglement slightly increases from the first pair with entanglement numbers $Z = 8$ and 12 to the second pair with $Z = 12$ and 18, but quickly decreases with increasing entanglement number when $Z > 12$. This trend is consistent with the experimental results if we consider that $Z = 8$ falls into the transient regime from Ogston-like to reptation migration and all larger chains are in the reptation regime. Due to the lack of a systematic experimental studies of electrophoresis of ssDNA with sizes larger than 1000 base pairs, we cannot give any direct comparison of theory to the experiment in this paper, but our predictions might be tested in the future by running a series of long-chain ssDNA molecules under conditions corresponding to those used for our simulations.

3 Concluding remarks

We have successfully simulated ssDNA electrophoretic behavior for a series of electric field strengths using our temporary network model based on coarse-grained Brownian dynamics, which shows a smooth transition from the reptation regime to the oriented reptation regime. The simulated results can be fitted with an interpolation equation having the same form as for dsDNA electrophoresis [13], but with different parameters. To use our simulations to predict mobilities, the chain size needs to fall within the reptation or oriented reptation regimes. In addition, the model is only applicable to DNA molecules whose length is much greater than the pore size so that the chain has multiple entanglements with the network.

For small values of entanglement number ($Z < 30$), our simulation results show a steeper slope than theoretically predicted (-1) or seen in experiments (varying from -0.3 to -0.7 for different gel/polymer concentrations). When $Z > 10$, the simulated mobility *versus* molecular size at low fields can be fitted by an asymptote equation composed of two terms: one is an exponential decay and the other a power law (Z^{-1}). As the formula (Eq. 17) predicts, the quick dissipation of the exponential decay functions in Eq. (17) may eventually lead to a function of $\tilde{\mu} \propto Z^{-1}$ for an infinite Z. Future simulations with $Z > 30$ may be done to check if this interpolation function is still valid for longer ssDNA chains.

The simulation results are in reasonably good agreement with experimental data when we use somewhat modified scaling factors to convert the dimensionless to dimensional parameters. Our work suggests that estimates of pore size or tube diameter and equilibrium time (τ_e) need to be carefully re-evaluated as functions of the sieving media.

Estimates of these quantities present the greatest source of uncertainty in comparing predicted and measured electrophoretic mobilities. We have also derived the peak widths from the SD of mobility by using the central limit theorem, and find a good agreement with the experimental peak widths, after converting dimensionless to dimensional values.

Since N_e represents the number of Kuhn steps *per* pore, the larger N_e is, the fewer entanglements one chain (of fixed length) has with the network at fixed Kuhn step length. Thus, a larger value of N_e should lead to a larger mobility for a fixed chain length (constant N but smaller Z); this means that the same size ssDNA molecule migrates faster in a gel of lower concentration with bigger pores. On the other hand, both the entanglement number Z and the chain length L can be held fixed while varying N_e by changing the pore size a and Kuhn step length b_K (by changing ionic strength) in such a way that $a \propto b_K^2$. Also in real gels, the distribution in pore sizes or tube diameters would presumably result in a changing N_e and Z for each chain as it moves through the gel. In the future, a spatially varying average tube diameter could be introduced to account for this heterogeneity of the network.

A limitation of our model is the assumption that the persistence length of the DNA molecule is smaller than the pore size, which fails for densely cross-linked gels. In addition, the model is only applicable to DNA molecules whose length is much greater than the pore size so that the DNA molecule has multiple entanglements with the gel. This assumption fails for short ssDNA molecules which interact with the gel by Ogston-like sieving. We also neglect constraint-release due to motion of the molecules in the sieving medium.

4 References

[1] Schieber, J. D., Neergaard, J., Gupta, S., *J. Rheol.* 2003, *47*, 213–233.

[2] Semenov, A. N., Duke, T. A., Viovy, J., *Phys. Rev. E Stat. Phys. Plasmas Fluids Relat. Interdiscip. Topics* 1995, *51*, 1520–1537.

[3] Duke, T., Viovy, J. L., Semenov, A. N., *Biopolymers* 1994, *34*, 239–247.

[4] Duke, T. A., *Phys. Rev. Lett.* 1989, *62*, 2877–2880.

[5] de Gennes, P. G., *J. Chem. Phys.* 1971, *55*, 572–579.

[6] Doi, M., Edwards, S. F., *The Theory of Polymer Dynamics*, Oxford University Press, New York 1986.

[7] Slater, G. W., Noolandi, J., *Biopolymers* 1986, *25*, 431–454.

[8] Barkema, G. T., Marko, J. F., Widom, B., *Phys. Rev. E Stat. Phys. Plasmas Fluids Relat. Interdiscip. Topics* 1994, *49*, 5303–5309.

[9] van Heukelum, A., Barkema, G. T., *Electrophoresis* 2002, *23*, 2562–2568.

[10] Heukelum, V. A., Beljaars, H. R. W., *J. Chem. Phys.* 2000, *113*, 3909–3915.

[11] Smith, S. B., Heller, C., Bustamante, C., *Biochemistry* 1991, *30*, 5264–5274.

[12] Zimm, B. H., *J. Chem. Phys.* 1991, *94*, 2187–2206.

[13] Graham, R. S., Larson, R. G., *Macromolecules* 2007, *40*, 366–378.

[14] Oda, R. P., Landers, J. P., *Handbook of Capillary Electrophoresis*, CRC Press, Boca Raton, FL 1997, pp. 2–42.

[15] Heller, C., *Electrophoresis* 1998, *19*, 3114–3127.

[16] Wang, Y., Liang, D., Ying, Q., Chu, B., *Electrophoresis* 2005, *26*, 126–136.

[17] Zhou, H., Miller, A. W., Sosic, Z., Buchholz, B. *et al.*, *Anal. Chem.* 2000, *72*, 1045–1052.

[18] Manabe, T., Chen, N., Terabe, S., Yohda, M., Endo, I., *Anal. Chem.* 1994, *66*, 4243–4252.

[19] Slater, G. W., Drouin, G., *Electrophoresis* 1992, *13*, 574–582.

[20] Cohen, A., *Rheol. Acta* 1991, *30*, 270–273.

[21] Tinland, B., Pluen, A., Sturm, J., Weill, G., *Macromolecules* 1997, *30*, 5763–5765.

[22] Mohanty, U., Stellwagen, N. C., *Biopolymers* 1999, *49*, 209–214.

[23] Smith, S. B., Bendich, A. J., *Biopolymers* 1990, *29*, 1167–1173.

[24] Smith, S. B., Finzi, L., Bustamante, C., *Science* 1992, *258*, 1122–1126.

[25] Record, M. T., Jr., Anderson, C. F., Lohman, T. M., *Q. Rev. Biophys.* 1978, *11*, 103–178.

[26] Oberthur, R. C., *Makromol. Chem.* 1978, *179*, 2693–2706.

[27] Fabrizio, E. F., Nadim, A., Sterling, J. D., *Anal. Chem.* 2003, *75*, 5012–5021.

[28] Nkodo, A. E., Garnier, J. M., Tinland, B., Ren, H. *et al.*, *Electrophoresis* 2001, *22*, 2424–2432.

[29] Hoagland, D. A., Arvanitidou, E., Welch, C., *Macromolecules* 1999, *32*, 6180–6190.

[30] Volkel, A. R., Noolandi, J., *Macromolecules* 1995, *28*, 8182–8189.

[31] Stellwagen, E., Stellwagen, N. C., *Electrophoresis* 2002, *23*, 2794–2803.

[32] Desruisseaux, C., Long, D., Drouin, G., Slater, G. W., *Macromolecules* 2001, *34*, 44–52.

[33] Rousseau, J., Drouin, G., Slater, G. W., *Electrophoresis* 2000, *21*, 1464–1470.

[34] Stellwagen, N. C., Gelfi, C., Righetti, P. G., *Biopolymers* 1997, *42*, 687–703.

[35] Tanford, C., *Physical Chemistry of Macromolecules*, Wiley, New York 1961, p. 710.

[36] Chui, M. M., Phillips, R. J., McCarthy, M. J., *J. Colloid Interface Sci.* 1995, *174*, 336–344.

[37] Ferguson, K. A., *Metabolism* 1964, *13*, 985–1002.

[38] Stellwagen, N. C., *Electrophoresis* 1998, *19*, 1542–1547.

[39] Viovy, J. L., *Rev. Modern Phys.* 2000, *72*, 813–872.

[40] Holmes, D. L., Stellwagen, N. C., *Electrophoresis* 1991, *12*, 612–619.

[41] Zhao, Q., Chen, W., Zhu, Q., *Mater. Lett.* 2003, *57*, 1756–1758.

[42] Doherty, E. A., Kan, C. W., Paegel, B. M., Yeung, S. H. *et al.*, *Anal. Chem.* 2004, *76*, 5249–5256.

[43] Wu, C., Quesada, M. A., Schneider, D. K., Farinato, R. *et al.*, *Electrophoresis* 1996, *17*, 1103–1109.

[44] Gennes, P.-G. D., *Introduction to Polymer Dynamics*, Cambridge University Press, Cambridge, New York 1990.

[45] Slater, G. W., Kenward, M., McCormick, L. C., Gauthier, M. G., *Curr. Opin. Biotechnol.* 2003, *14*, 58–64.

[46] Schurr, J. M., Schmitz, K. S., *Ann. Rev. Phys. Chem.* 1986, *37*, 271–305.

[47] Pluen, A., Tinland, B., Sturm, J., Weill, G., *Electrophoresis* 1998, *19*, 1548–1559.

[48] Todorov, T. I., Morris, M. D., *Electrophoresis* 2002, *23*, 1033–1044.

[49] Volkmuth, W. D., Duke, T., Wu, M. C., Austin, R. H., Szabo, A., *Phys. Rev. Lett.* 1994, *72*, 2117–2120.

[50] Lo, R. C., Ugaz, V. M., *Electrophoresis* 2006, *27*, 373–386.

5 Appendix

Decorrelation and SD

The velocity autocorrelation coefficient can be used to determine how widely in time we must space our sampling of mobility values to ensure that these mobilities are statistically independent. The mobility values were simulated by recording the mass center positions of the chain every 500 time steps (*i.e.* $\widetilde{t}_s = 5$) and then dividing the position change projected in the field direction by the sampling time interval duration $\widetilde{t}_s$. The mobility time–auto correlation function $R(h)$ (Eq. A1) is a function of the number of time intervals of duration $\widetilde{t}_s$. Thus, $h = 1$ corresponds to a time period of $\widetilde{t}_s$, $h = 2$ corresponds to $2\,\widetilde{t}_s$, *etc.* If we define μ_i to be the mobility averaged over the ith time interval of duration $\widetilde{t}_s$, and μ_{i+h} is the mobility value averaged over the $(i + h)$th time interval, then the autocorrelation coefficient R is defined as in Eq. (A1).

$$R(h) = \frac{C_h}{C_o} \tag{A1}$$

where

$$C_h = \frac{1}{N-h}\sum_{t=1}^{N-h}(\mu_t - \bar{\mu})(\mu_{t+h} - \bar{\mu}),$$

$$C_0 = \frac{\sum_{t=1}^{N}(\mu_t - \bar{\mu})^2}{N}$$

In Fig. 11, the mobility autocorrelation function decays to less than 5% correlation at $h \geq 1$ (except when $\varepsilon = 1$). Thus, if the values of the mobility are each averaged over a time interval of $\widetilde{t}_s$ (*i.e.*, $h = 1$), and separated in time by this same interval, then these values can be considered to be nearly independent of each other and can be used to determine the variance of the mobility. From the mobility variance, we can construct a plot of DNA molecular migration and band broadening *versus* separation distance by using the mean and SD of mobility. The assumption for this construction is that DNA molecules follow a Gaussian distribution of mobility as they disperse during their migration, which should be valid for a gel of uniform properties, according to the central limit theorem.

While the time autocorrelation indicates that there should be no significant correlation between our mobility values, we can test this further by seeing if the SD σ of the mobilities is inversely proportional to the square root of the interval over which each mobility value is averaged. This can be tested by averaging together each block of N sequential values of the mobilities and then computing the SD of the resulting (N-fold fewer) "consolidated" mobilities. The result $\sigma \propto 1/\sqrt{N}$ will be obtained if there is no correlation in the series of mobility values. The power law fit in Fig. 12 shows that the SD is proportional to the number of mobility values consolidated into a single value raised to a power of -0.47 ± 0.013. The closeness of this value to -0.5 indicates the validity of using our mobility data to calculate the SD of mobility and peak width. As expected, the standard error is insensitive to the consolidation number, since the standard error equals the SD divided by the square root of the number of data points minus one, and the number of data points decreases inversely with the consolidation number. Hence, for the standard error, the decrease in SD is cancelled by the decrease in the number of consolidated points.

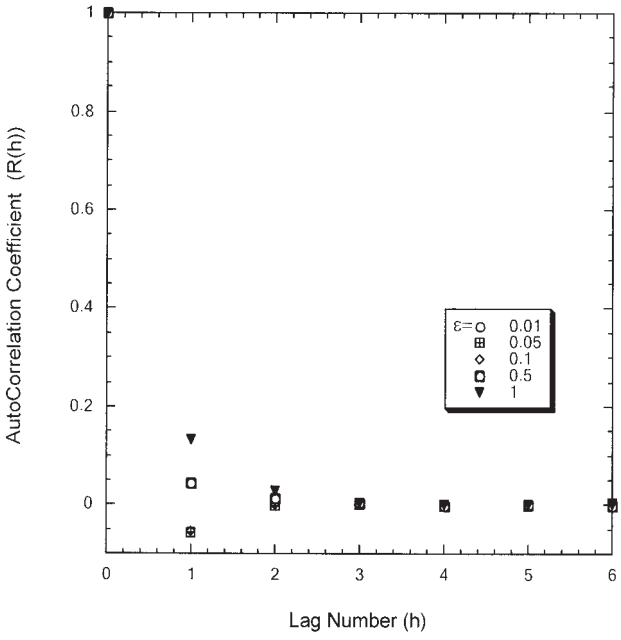

Figure 11. Plots of autocorrelation coefficient *vs.* number of lag times, each of duration $\widetilde{t}_s = 5$ for various reduced field strengths ε for a DNA chain with six entanglements. The simulation timestep was $\Delta\widetilde{t} = 0.01$.

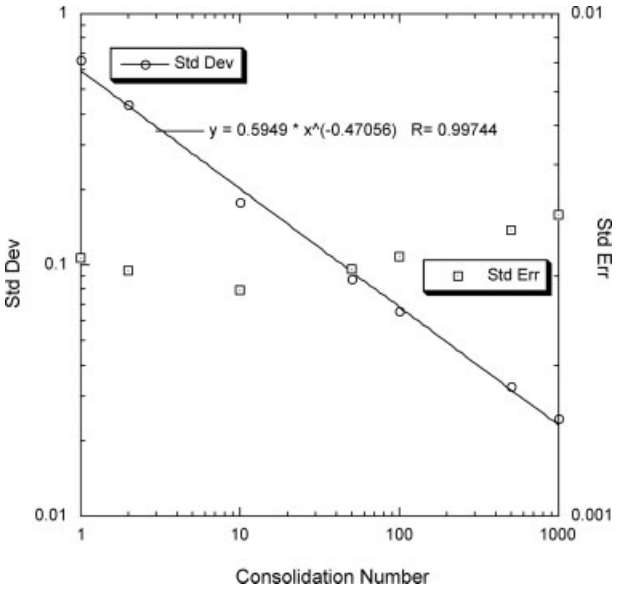

Figure 12. SD and standard error for simulated DNA chain with $Z = 24$ at reduced field $\varepsilon = 0.1$. The "consolidation number" is the number of time intervals (each of length $\tilde{t}_s = 5$) that each mobility value is averaged over.

